Phase transitions of a few-electron system in a spherical quantum dot

P. A. Sundqvist,[1,*] S. Yu. Volkov,[2] Yu. E. Lozovik,[2] and M. Willander[1]
[1]*Laboratory of Physical Electronics and Photonics, MC2, Department of Physics, University of Gothenburg and Chalmers University of Technology, Fysikgränd 3, S-412 96 Gothenburg, Sweden*
[2]*Institute of Spectroscopy, 142190 Moscow Region, Troitsk, Russia*
(Received 26 December 2001; revised manuscript received 3 June 2002; published 29 August 2002)

The spin configurations of a spherical quantum dot, defined by a three-dimensional (3D) harmonic confinement potential, containing a few Coulomb Fermi particles (electrons or holes) are studied. Quantum transitions involving a spin transformation and a ''cold melting'' (from a Wigner crystal-like state, i.e., from regime of strongly correlated electrons, to a Fermi-liquid-like phase) is driven by the dimensionless quantum control parameter q (which is connected with steepness of the confinement potential) is demonstrated. The pair correlation and radial distribution functions which characterize electronic quantum delocalization are analyzed. The calculations using the unrestricted variational Hartree-Fock method (for the ground state at $T=0$ K) and the more computer intensive quantum path integral Monte Carlo method (for $T\neq 0$ K) are performed and compared. For small q, the ground state of the three electron system is crystal-like and has C_3 symmetry, i.e., the maxima of electron density are located at the nodes of an equilateral triangle. The preferable spin configuration for small q is ''ferromagnetic,'' with total spin $S=3/2$. As q rises, the widths of the one-electron wave functions grow and become overlapping. At a critical value q_1 the ground state changes from $S=3/2$ to $S=1/2$ and at the same time, asymmetry appears in the triangle (i.e., spontaneous breaking of the C_3 symmetry to C_2 symmetry). At a second critical value q_2 the electron distribution undergoes a symmetry phase transition, from trianglelike (with C_2 symmetry) to axial symmetric (with C_∞ symmetry). As q grows further, we obtain a Fermi-liquid-like (non-interacting) electron configuration in the ground state ($S=1/2$). In addition, the $S=3/2$ state, at a critical q value (which is slightly larger than q_1) undergoes a dramatic charge redistribution.

DOI: 10.1103/PhysRevB.66.075335 PACS number(s): 73.61.−r, 02.70.Rr, 05.30.Fk

I. INTRODUCTION

The behavior of a many-electron system in a quantum dot is of great interest, especially in the regime of strongly correlated electrons.[1–7] This can be achieved for rarefied electron systems by the change of a confinement parameter, for example, using a controlling gate,[8,9] or by using a normal magnetic field.[10] This possibility distinguishes quantum dots—giant artificial atoms—from natural atoms with rather weakly correlated electrons (in all natural atoms the total correlation energy is always smaller than the Hartree-Fock energy). Therefore, detailed analysis of all quantum dot characteristics in a wide range of the dimensionless quantum parameter q (connected with the steepness of the confining potential and hence control of the correlation of the electrons) is important, particularly the study of electron crystallization and quantum ''cold'' melting. In addition, spin transformation driven by a change of the confinement potential is interesting in connection with phenomena such as spin blockades and also for spin memory applications.

In this paper we study in detail the behavior of a few-electron quantum system inside a spherical quantum dot with parabolic confinement. The model is equivalent to a quantum analog of the three-dimensional (3D) Thomson atom (see, for example, Ref. 1 and references therein). All properties of the system at sufficiently low temperatures depend only on the dimensionless quantum parameter q, which is connected with the steepness of the confinement potential. We therefore analyze how the properties of the spherical quantum dot depend on q and the total spin. We have studied the following characteristics of the few-electron system in the quantum dot: radial and pair distribution functions and total and exchange energies. We also analyze the symmetry of the electron configuration and the effect of the Fermi statistics on the behavior of the quantities under consideration. We use *unrestricted* variational Hartree-Fock (HF) and *ab initio* quantum path integral Monte Carlo (PIMC) methods for fermions.

These two methods are complementary. First, the HF method requires assumptions about the symmetry of the system to be made, which is justified by the PIMC results. Second the HF method as shown below allows more precise calculations to be performed (in the region of small confinement strength) and requires much less central processing unit (CPU) time.

In Sec. II the model of a spherical quantum dot is presented. In Sec. III the results of the unrestricted Hartree-Fock approximation are analyzed. In Sec. IV the results obtained by the path integral Monte Carlo calculation are described. Section V is devoted to a summary and conclusions.

II. MODEL OF A FEW-ELECTRON SYSTEM

We use a three-dimensional parabolic confinement as a spherical quantum dot model. Such a confinement describes real quantum dots with small number of electrons.[11,12] The Hamiltonian of the system is

$$H=\sum_{i=1}^{N}\frac{-\hbar^2}{2m}\nabla_i^2+\sum_{i=1}^{N}\frac{m\omega^2}{2}r_i^2+\sum_{i<j}^{N}\frac{e^2}{\epsilon|r_i-r_j|}, \qquad (1)$$

where m is an effective electron mass and ϵ is the dielectric susceptibility. We use dimensionless variables for length, en-

ergy, and temperature: $r'=r/r_0$, $E'=E/E_0$, $T'=T/E_0$. Units of length and energy are $r_0=(2e^2/\epsilon m\omega^2)^{1/3}$, $E_0=e^2/\epsilon r_0=m\omega^2 r_0^2/2$. After these transformations the Hamiltonian takes the form

$$H=-\sum_i^N q\nabla_i^2+\sum_i^N r_i^2+\sum_{i<j}^N \frac{1}{r_{ij}}, \tag{2}$$

where $q=(\hbar^2/2m)(m\omega^2\epsilon^4/2e^8)^{1/3}$ is the dimensionless quantum control parameter of the system. It is easy to show that q can be expressed as the ratio of the effective Bohr radius $a_B^*=\hbar^2\varepsilon/m^*e^2$ and the one-particle length $l=(\hbar/m^*\omega)^{1/2}$ (of the ground state in the confinement potential) as $q=(a_B^*/2l)^{4/3}$. The controlling parameter q can also be expressed as the dimensionless ratio of the effective Bohr radius to the equilibrium interelectron distance r_0 in a classical cluster or as the dimensionless ratio of the characteristic quantum kinetic energy $\hbar/2m{r_0}^2$ to the characteristic classical Coulomb interaction $e^2/\epsilon r_0$. As an example we give some typical values for electrons in GaAs. At $\log_{10}(q)=-1.5$, we have $r_0=164$ nm, $l=69$ nm, and $E_0=0.67$ meV. More examples are given in Sec. III. The spin-dependent contributions (Breit's interaction and the spin-orbit interaction or the so-called LS coupling) are relatively small in the whole region of q. Furthermore, we will study the behavior of the system characteristics in the dependence on the dimensionless parameter q. q can be changed experimentally by controlling the steepness of the confining potential ω using a gate.

III. UNRESTRICTED HF VARIATIONAL APPROACH: THEORY AND RESULTS

There are several effective methods for treating the problem under consideration.[1–7,11–14] In this section we analyze the ground state of the problem using the unrestricted variational Hartree-Fock approach to take into account a possible spontaneous breaking of spherical symmetry of the Hamiltonian given by Eq. (2). We take three Gaussians as one-particle wave functions for the system of $N=3$ electrons. These Gaussians are centered at the corners (nodes) of a triangle in the x-y plane. The width of the Gaussians is controlled by a variational parameter σ, which is identical for all the functions. Hence the basis functions $\phi_i(\vec{r})$ are given by

$$\phi_i(\vec{r})=Ne^{-(1/2)[(x-x_{0,i})/\sigma]^2}e^{-(1/2)[(y-y_{0,i})/\sigma]^2}e^{-(1/2)(z/\sigma)^2}. \tag{3}$$

Note that the basis functions are nonorthogonal. There are three possibilities for arrangement of the three nodes $\vec{r}_{0,i}$ of a triangle with different symmetries, C_3, C_2, and C_∞, and they are plotted in Fig. 1. The node coordinates can be represented in the form

$$x_{0,1}=a,$$

$$y_{0,1}=0,$$

$$x_{0,2}=a-\frac{1}{2}\sqrt{4b_1^2-b_2^2},$$

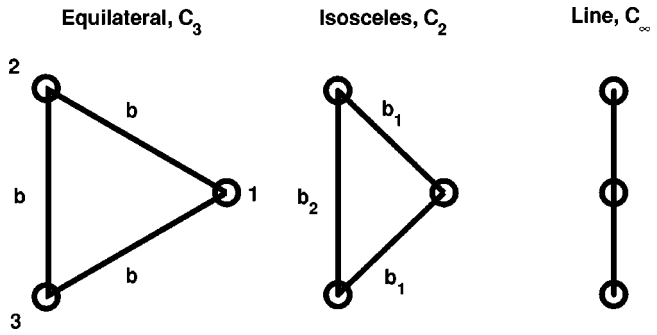

FIG. 1. Different realizations of symmetry with the given Gaussian basis set.

$$y_{0,2}=b_2/2,$$

$$x_{0,3}=a-\frac{1}{2}\sqrt{4b_1^2-b_2^2},$$

$$y_{0,3}=-b_2/2. \tag{4}$$

The center of mass and relative motions can be separated for parabolic confinement (see, e.g., Ref. 1). The center of mass oscillates as a 3D harmonic oscillator. Here we are interested in the relative electron configurations. The parameter a fixes the center of mass position and the electron configuration does not depend on a. We suppose for simplicity (and this is in agreement with the results of the quantum Monte Carlo simulation; see Sec. IV) that the triangle has at least C_2 symmetry relative to the x axis. It is easy to show that in the classical case, $b_1=b_2$, i.e., electrons are at the nodes of an equilateral triangle. It is obvious that the symmetry C_3 must be true also a for quantum system at sufficiently small q. When all the centers of Gaussians are on the same axis, i.e., $b_1=b_2/2$, we have an electron molecule with C_∞ symmetry. Below we shall show that all these cases (see Fig. 1) occur at different regions of the controlling parameter q.

The wave function of the system can be modeled by the eigenstates of the total spin S:

$$\left|\sum_{j=1}^3 \hat{\vec{S}}_j\right|^2\vec{\Psi}=S(S+1)\vec{\Psi}. \tag{5}$$

The spin operators act on the spinor with $2^3=8$ components:[15,16]

$$\vec{\Psi}=\begin{bmatrix}\Psi_{\uparrow,\uparrow,\uparrow}(\vec{r}_1,\vec{r}_2,\vec{r}_3)\\ \Psi_{\uparrow,\uparrow,\downarrow}(\vec{r}_1,\vec{r}_2,\vec{r}_3)\\ \Psi_{\uparrow,\downarrow,\uparrow}(\vec{r}_1,\vec{r}_2,\vec{r}_3)\\ \Psi_{\uparrow,\downarrow,\downarrow}(\vec{r}_1,\vec{r}_2,\vec{r}_3)\\ \Psi_{\downarrow,\uparrow,\uparrow}(\vec{r}_1,\vec{r}_2,\vec{r}_3)\\ \Psi_{\downarrow,\uparrow,\downarrow}(\vec{r}_1,\vec{r}_2,\vec{r}_3)\\ \Psi_{\downarrow,\downarrow,\uparrow}(\vec{r}_1,\vec{r}_2,\vec{r}_3)\\ \Psi_{\downarrow,\downarrow,\downarrow}(\vec{r}_1,\vec{r}_2,\vec{r}_3)\end{bmatrix}. \tag{6}$$

$\vec{S}^2$ is a constant 8×8 matrix that acts on the spinor given in Eq. (6). The equation responsible for spin effects [apart from Eq. (5)] is the total antisymmetry rule (for fermions), and is in general given by

$$\Psi_{s_1,\ldots s_i,\ldots s_j,\ldots s_N}(\vec{r}_1,\ldots\vec{r}_i,\ldots,\vec{r}_j,\ldots\vec{r}_N) = -\Psi_{s_1,\ldots s_j,\ldots s_i,\ldots s_N}(\vec{r}_1,\ldots\vec{r}_j,\ldots,\vec{r}_i,\ldots\vec{r}_N). \tag{7}$$

For the ''ferromagnetic'' state with total spin $S=3/2$ we have a fourfold degeneracy with respect to S_z. Their waveforms are exactly equal and we give here the expression for $S_z=+3/2$, where only the component $\Psi_{\uparrow,\uparrow,\uparrow}$ is not equal to zero and is fully antisymmetrical:

$$\Psi_{\uparrow,\uparrow,\uparrow}(\vec{r}_1,\vec{r}_2,\vec{r}_3)=\begin{vmatrix}\phi_1(\vec{r}_1) & \phi_1(\vec{r}_2) & \phi_1(\vec{r}_3)\\ \phi_2(\vec{r}_1) & \phi_2(\vec{r}_2) & \phi_2(\vec{r}_3)\\ \phi_3(\vec{r}_1) & \phi_3(\vec{r}_2) & \phi_3(\vec{r}_3)\end{vmatrix}. \tag{8}$$

For the completion we also consider the ''antiferromagnetic'' state with $S=1/2$. The total spin constriction $S=1/2$ in Eq. (5) (giving $\Psi_{\uparrow,\uparrow,\downarrow}=-f_1-f_2$, $\Psi_{\uparrow,\downarrow,\uparrow}=f_2$ and $\Psi_{\downarrow,\uparrow,\uparrow}=f_1$, where f_1 and f_2 are arbitrary functions of the coordinates) and Eq. (7) with the particle permutations $1\rightleftharpoons 2$, $1\rightleftharpoons 3$, and $2\rightleftharpoons 3$ will restrict the waveform of the spinor components (f_1 and f_2). Since the solution of $S=1/2$ is degenerate with respect to S_z, we give here a waveform on the components $\Psi_{\uparrow,\uparrow,\downarrow}$, $\Psi_{\uparrow,\downarrow,\uparrow}$, and $\Psi_{\downarrow,\uparrow,\uparrow}$ (all with $S_z=+1/2$) as:

$$\Psi_{\uparrow,\uparrow,\downarrow}(\vec{r}_1,\vec{r}_2,\vec{r}_3)=\frac{1}{3}\phi_1(\vec{r}_3)\begin{vmatrix}\phi_2(\vec{r}_1) & \phi_2(\vec{r}_2)\\ \phi_3(\vec{r}_1) & \phi_3(\vec{r}_2)\end{vmatrix}+\frac{1}{6}\phi_1(\vec{r}_2)\begin{vmatrix}\phi_2(\vec{r}_1) & \phi_2(\vec{r}_3)\\ \phi_3(\vec{r}_1) & \phi_3(\vec{r}_3)\end{vmatrix}+\frac{1}{6}\phi_1(\vec{r}_1)\begin{vmatrix}\phi_2(\vec{r}_3) & \phi_2(\vec{r}_2)\\ \phi_3(\vec{r}_3) & \phi_3(\vec{r}_2)\end{vmatrix}, \tag{9}$$

$$\Psi_{\uparrow,\downarrow,\uparrow}(\vec{r}_1,\vec{r}_2,\vec{r}_3)=\frac{1}{3}\phi_1(\vec{r}_2)\begin{vmatrix}\phi_2(\vec{r}_1) & \phi_2(\vec{r}_3)\\ \phi_3(\vec{r}_1) & \phi_3(\vec{r}_3)\end{vmatrix}+\frac{1}{6}\phi_1(\vec{r}_1)\begin{vmatrix}\phi_2(\vec{r}_2) & \phi_2(\vec{r}_3)\\ \phi_3(\vec{r}_2) & \phi_3(\vec{r}_3)\end{vmatrix}+\frac{1}{6}\phi_1(\vec{r}_3)\begin{vmatrix}\phi_2(\vec{r}_1) & \phi_2(\vec{r}_2)\\ \phi_3(\vec{r}_1) & \phi_3(\vec{r}_2)\end{vmatrix}, \tag{10}$$

$$\Psi_{\uparrow,\downarrow,\downarrow}(\vec{r}_1,\vec{r}_2,\vec{r}_3)=\frac{1}{3}\phi_1(\vec{r}_1)\begin{vmatrix}\phi_2(\vec{r}_2) & \phi_2(\vec{r}_3)\\ \phi_3(\vec{r}_2) & \phi_3(\vec{r}_3)\end{vmatrix}+\frac{1}{6}\phi_1(\vec{r}_2)\begin{vmatrix}\phi_2(\vec{r}_1) & \phi_2(\vec{r}_3)\\ \phi_3(\vec{r}_1) & \phi_3(\vec{r}_3)\end{vmatrix}+\frac{1}{6}\phi_1(\vec{r}_3)\begin{vmatrix}\phi_2(\vec{r}_1) & \phi_2(\vec{r}_2)\\ \phi_3(\vec{r}_1) & \phi_3(\vec{r}_2)\end{vmatrix}. \tag{11}$$

The total charge density is defined as the sum of the squared one-particle functions, but we prefer to define the reduced one-particle probability P_1 since the wave functions could overlap significantly. We now integrate out two coordinates. $\vec{r}_2$ and $\vec{r}_3$ were chosen; however, due to the total antisymmetry of the wave function [see Eq. (7)] any two could have been chosen. For the ''antiferromagnetic'' state it is given by

$$\begin{aligned}P_1(\vec{r}_1)&\equiv\sum_{j=1}^{8}\int d^3r_3\int d^3r_2|\Psi_j|^2\\ &=\frac{1}{3}\phi_1^2(1-J_2^2)+\frac{1}{6}(\phi_2^2+\phi_3^2)(2+J_1^2)\\ &\quad+\frac{\phi_1}{3}(\phi_2+\phi_3)J_1(1-J_2)-\frac{1}{3}\phi_2\phi_3(J_1^2+2J_2)\end{aligned} \tag{12}$$

where the explicit coordinate dependence on the functions is omitted in the above expression. The definitions of J_1 and J_2 are given in the Appendix. For $J_1, J_2\to 0$ (small overlap) we obtain the ''classical'' total charge density and for $J_1, J_2 \to 1$ P_1 cancels due to Pauli's exclusion principle. Notice that P_1 is mirror symmetric around the x axis (see Fig. 1). The expressions for energies $\langle H\rangle$, and both the ''ferromagnetic'' and ''antiferromagnetic'' states as functions of the variational parameters b and σ are presented in the Appendix.

First we analyze the ferromagnetic state $|\uparrow\uparrow\uparrow\rangle$, $S=3/2$. From the expressions given in the Appendix it follows that if q is small enough and there is only a small overlap of the basis functions (i.e., b/σ is large), we can approximate $\langle H\rangle$ as

$$E_{\text{appr}}=\frac{9q}{2\sigma^2}+\frac{3\sigma^2}{2}\left[3+\frac{2}{3}\left(\frac{b}{\sigma}\right)^2\right]+\frac{3}{b}. \tag{13}$$

If we minimize the energy with respect to b and σ, we find that the local minimum occurs when

$$b_0=\left(\frac{3}{2}\right)^{1/3}, \tag{14}$$

$$\sigma_0=q^{1/4}. \tag{15}$$

Substituting these values into Eq. (13) yields the ground-state energy:

$$E_0=3\left(\frac{3}{2}\right)^{2/3}+9\sqrt{q}. \tag{16}$$

The square root dependence corresponds to the harmonic confinement energy.

Now we analyze the transformation of electron configuration in the ferromagnetic state driven by the quantum control parameter q. In Fig. 2 a contour plot of the total energy is shown as a function of b and σ at $q=0.053$. At this value we obtain a bistable global solution. The two minima (indicated by ○ and + in the figure) have the same energy. We denote this critical value of q by q_c. When $q<q_c$, the global minimum corresponds to the ○, corresponding to the ''classical'' minimum. By the classical minimum we mean the Wigner-crystal-like configuration of charges where the total potential energy dominates the Hamiltonian. Strictly speaking this is the case when $b=b_0$. For $q>q_c$ the quantum kinetic contributions will be important, and as a result, the ''condensed'' minima marked with a + have lower energy.

In Fig. 3, the result of the minimization is plotted as a function of $\log_{10}(q)$. Notice that the transition is very sharp at $q=q_c$. The change in b and σ is actually infinetely sharp at $T=0$. However, at finite temperature the transition will be continuous and the fermions will be in a superposition of the ○ state and the + state. After the transition the value of b is reduced by a factor of 5. The top figure shows E_1-E_2 as a function of q. When E_1-E_2 crosses the zero axis the ground state changes from the ○ state to the + state. It is interesting to note that the control parameter q, plays a role analogous to the temperature in the Ginzburg-Landau theory for superconductors.

After the phase transition point, the overlap integral J, which is defined in the Appendix, takes an almost constant value of 0.97. In the range $-3<\log_{10}(q)<-1.2758$, the overlap increases exponentially up to this limit, with the kink at $\log_{10}(q)\approx-2$. Since the overlap is large, the exchange energy will also be large. The exchange energy is defined here as the difference between the ground-state energy and the corresponding unrestricted Hartree energy (with the same values of b and σ). After the transition point the exchange energy increases from -5% of the ground-state energy up to $+22\%$, while J is almost constant. This shows that the exchange plays an important role in the phase transition.

In Fig. 4, the probability distribution for one electron is plotted for $q<q_c$ and $q>q_c$ for the region near corners of the triangle (the others follow from total antisymmetry) and shows the C_3 symmetry clearly. The contour plot shows that the triangular Gaussian distribution at $q=q_c$ suddenly condenses to one central but wider peak.

Now we analyze the antiferromagnetic state and compare its energy with the ferromagnetic case to look for a global minimum, i.e., for a ground state. We find its energy by the minimization of $\langle H\rangle$ using expressions in the Appendix. The result shows that at $\log_{10}(q_1)<-1.3077$, the energy is minimal for the ''ferromagnetic'' state $S=3/2$ and otherwise the antiferromagnetic state $|\uparrow\uparrow\downarrow\rangle$ is favorable. The structural condensation phase transition takes place after the spin transition. The energy difference between the ferromagnetic and the antiferromagnetic state is, however, small for small q. In Fig. 5, the energy difference (absolute value) between $S=3/2$ and $S=1/2$ is converted to real temperature for a GaAs system in a logarithmic scale. The figure also shows typical sizes of the electron molecule at some values of q. For $q<q_1$ (indicated with a line in the figure) the system is ferromagnetic. From this figure we can estimate the temperature needed to destroy the ferromagnetism.

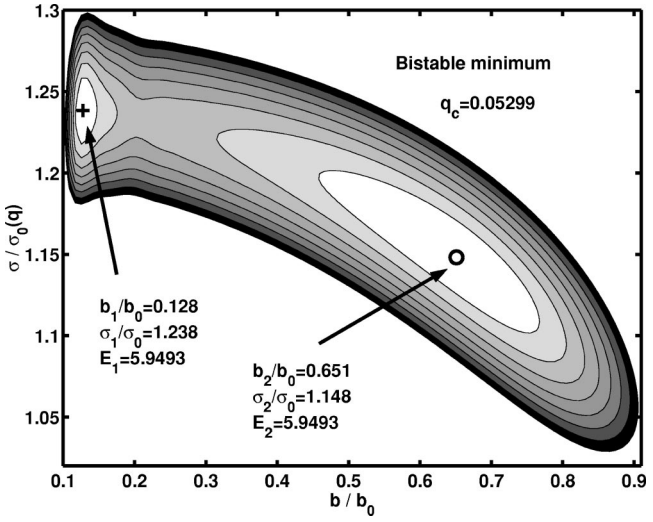

FIG. 2. Contour plot of energy vs minimization parameters b and σ at the critical value $q=q_c=0.053$. At this value of q there is two global minima, here marked with + (condensed minimum) and ○ (minimum for normal Wigner cluster).

In Fig. 6, the result of the minimization is shown. The figure shows the second critical point q_2, where the symmetry phase transition $C_2\rightarrow C_\infty$ occurs. The ratio b_1/b_2 determines the symmetry of the system. When this ratio equals 1 we have C_3 symmetry. When $1>b_1/b_2>1/2$ we have C_2 symmetry, and finally when it equals 1/2 we have C_∞ symmetry. After the spin transition to the antiferromagnetic state we have C_2 symmetry but for $\log_{10}(q)>-1.2$ the ratio

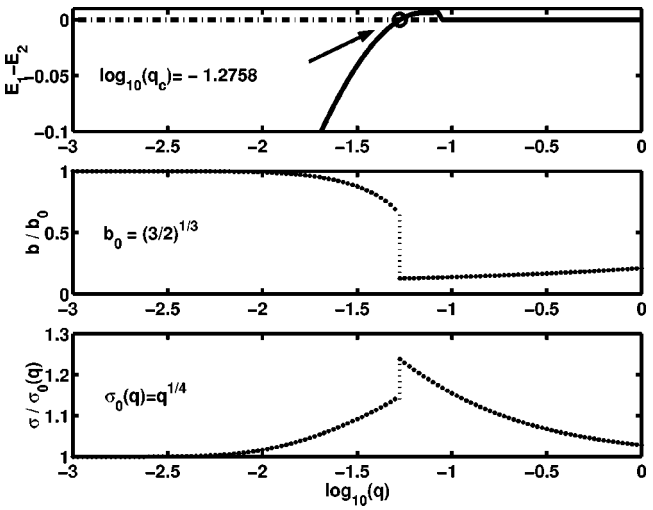

FIG. 3. Energy difference between classical E_1 and condensed minimum E_2 as a function of q for $S=3/2$ (top figure). Distance b in equilateral triangle (middle figure) vs q. Widths σ of one-electron wave functions (bottom figure) vs q. For q smaller than the critical condensation value q_c, the classical minimum is the ground state.

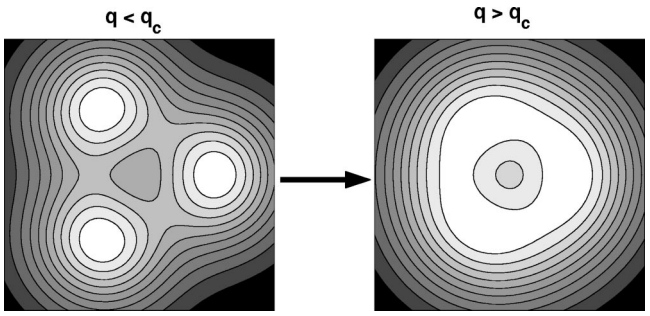

FIG. 4. Sequence of the total electron density at $z=0$ for $S=3/2$. The figure shows the electron configuration right before and after the transition (e.g., $q<q_c$ and $q>q_c$). The white area corresponds to maximal amplitude. Note the small local minimum in the condensed configuration.

b_1/b_2 decreases quickly towards 1/2. For $\log_{10}(q_2) > -0.772$ the ratio is 1/2, i.e., the system has C_∞ symmetry. Note that the derivatives of b_2 and σ are discontinuous at this point. As was shown above the symmetry C_∞ (which takes place for the Hamiltonian of the system) is restored at sufficiently large controlling parameter q. In Fig. 7, the probability distribution is plotted for four values of q, close to the transition region. It is interesting that spontaneous breaking of symmetry corresponds to that disappearance of the cluster crystallization, i.e., the quantum melting of the cluster. The figure shows clearly that the C_2 symmetry appears in an intermediate region of q. When $q>q_2$ (the bottom figure to the right in Fig. 7) the probability distribution has C_∞ symmetry. Only much later, at larger q when the Coulomb interactions become much smaller than the confinement is the electronic structure of the system identical to that of three noninteracting electrons in a parabolic confinement. Indeed, as one can easily show for the independent three electrons in the parabolic confinement potential, the ground state corresponds to the $1s^2 1p^1$ configuration (contrary to the configuration $1s^2 2s^1$ for the hydrogen atom); this is due to the expression for the energy of the spherical harmonic oscillator:

$$E_{n,l}=\hbar\omega\left(\frac{3}{2}+l+2n\right), \tag{17}$$

where $n=0,1,2,\ldots$, $l=0,1,2,\ldots$, and $\hbar\omega/E_0$ is equal to $2\sqrt{q}$. We stress that the electron configuration $1s^2 1p^1$ has the same C_∞ symmetry. Thus it is interesting and natural to compare the results of the unrestricted Gaussian HF method with those obtained by restricted HF method, with orbitals

$$\begin{aligned}\psi_{1s}&=N_{1s}e^{-(1/2)(r/\sigma_1)^2}Y_0^0(\theta,\varphi),\\ \psi_{1p}&=N_{1p}re^{-(1/2)(r/\sigma_2)^2}Y_1^0(\theta,\varphi),\end{aligned} \tag{18}$$

in the $1s^2 1p^1$ antiferromagnetic state $|\uparrow\uparrow\downarrow\rangle$. Doing the same procedure as above for the Gaussian antiferromagnetic case, we obtain an analytic expression for the energy as a function of σ_1 and σ_2, $E(\sigma_1,\sigma_2)$. Minimizing this with respect to the two variational parameters σ_1 and σ_2 then gives the global minimum. This energy is about 25% larger than the Gaussian energy for $\log_{10}(q)=-3$. The difference between the two

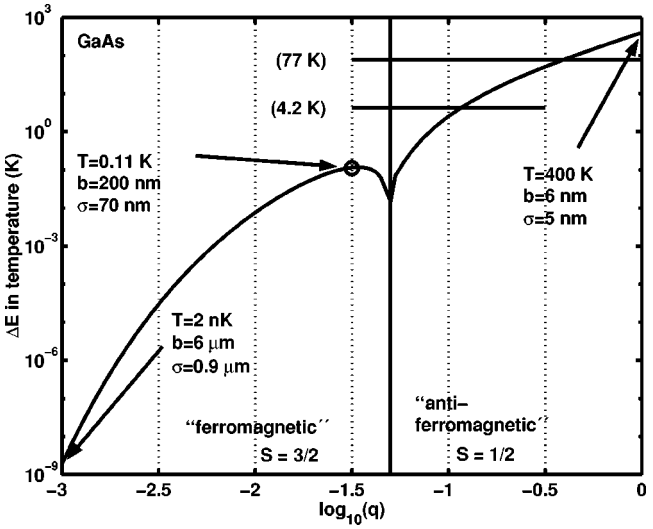

FIG. 5. Energy difference (absolute value) between $S=3/2$ and $S=1/2$ converted to temperature, for a GaAs system. To destroy the ferromagnetism in the dot, for $\log_{10}(q)=-1.5$ we need a temperature of 0.1 K. The typical dimensions of the system b and σ are also given at some points, as well as standard temperatures.

energies decreases as q increases. Starting from $\log_{10}(q) = -0.7258$ the restricted (atomiclike) HF function gives the best result. It differs, however, very little from the unrestricted Gaussian HF (with C_∞ symmetry) result, e.g., the correlation energy is small. The total electron density for the Gaussians aligned on the same axis (C_∞ symmetry) does look the same as that for the independent $1s^2 1p^1$ configuration, e.g.,

$$P_1(\vec{r})\cong 2\psi_{1s}^2(\vec{r})+\psi_{1p}^2(\vec{r}), \tag{19}$$

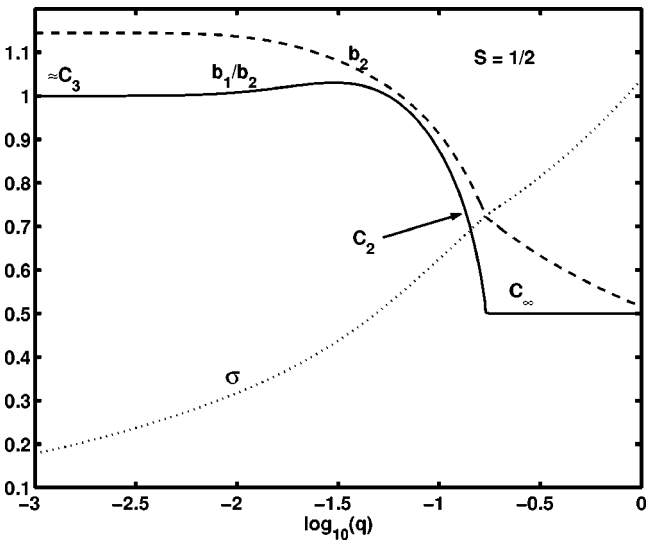

FIG. 6. Phase transition diagram for the antiferromagnetic state. The ratio b_1/b_2, b_2, and σ are plotted as a function of q. The ratio b_1/b_2 gives the symmetry information. Note the discontinuous derivative of b_2 and σ at $\log_{10}(q)=-0.772$. At this point we change from C_2 symmetry to C_∞ symmetry.

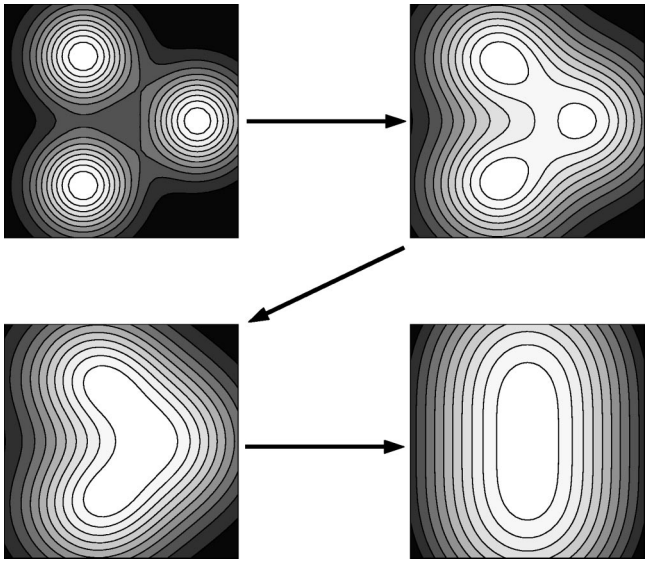

FIG. 7. A sequence of the one-particle probability at $z=0$ for the antiferromagnetic state. The sequence shows the gradual change of symmetry from C_3, C_2, to C_∞ (arrows indicate growing direction of controlling parameter q). For small q the width is small and the wave functions are not overlapping. For larger q the overlap becomes bigger. The final C_∞ symmetry is built up by Gaussians that are nearly equal to the total density of the $1s^2 1p^1$ configuration.

for large values of q [P_1 is defined in Eq. (12)]. However, this is not true for small values of q, as very many one-particle orbitals have to be used to satisfactorily build a Wigner crystal.

Finally we sum up the transition steps as follows: There are three critical values of q. Two of them, q_1 and q_2, refer to transitions within the ground state, and the third, q_c, refers to a transition in the ferromagnetic state. At $\log_{10}(q_c) = -1.2758$, we go from classical C_3 symmetry to condensed C_3 in the ferromagnetic state. At $\log_{10}(q_1) = -1.3077$ the system goes from a ferromagnetic state to an antiferromagnetic state (a spin transition) and at the same time from C_3 to C_2 symmetry. At $\log_{10}(q_2) = -0.772$ we obtain a sharp symmetry transition from C_2 symmetry to C_∞ symmetry. Up to this point Gaussians give a lower energy than the $1s^2 1p^1$ state. Even if it is not a fundamental transition, the ground state will, for $\log_{10}(q) > -0.7258$, be in the $1s^2 1p^1$ configuration state. They converge, however, in their characteristics for energy and one-particle probability. They both have C_∞ symmetry. We hence conclude that our choice of variational parameters in the Gaussian basis set is good, since it is sufficient to realize both the structure of a Wigner crystal and the independent (noninteracting) electron configuration. In Table I, the energy as a function of $\log_{10}(q)$ is listed for the ferromagnetic $S=3/2$ unrestricted variational HF state, the antiferromagnetic $S=1/2$ HF state, and the restricted atomic HF ($1s^2 1p^1$) state. The unrestricted variational HF method gives results in very good agreement with quantum MC results (compare the values in Table I with the results in Fig. 8).

TABLE I. Dimensionless energy E' for ferromagnetic HF, antiferromagnetic HF, and $1s^2 1p^1$ configuration (also antiferromagnetic) for different values of q. The ground state is labeled with an asterisk.

$\log_{10}(q)$	Ferro-magnetic HF	Antiferro-magnetic HF	$1s^2 1p^1$
−3.0	4.2157*	4.2157	5.2707
−2.5	4.4372*	4.4372	5.3092
−2.0	4.8272*	4.8302	5.4265
−1.5	5.4948*	5.5096	5.7655
−1.0	6.7346	6.6317*	6.6554
−0.5	9.3650	8.7131	8.7129*
−0.0	14.5763	12.9503	12.9502*

IV. THE PIMC SIMULATION

A. Description of the PIMC method and calculated properties

In this section we describe the path integral Monte Carlo simulations that were performed. In these calculations the Fermi statistics were included by considering the particle trajectory and permutations in ''imaginary time'' (see, for example, Ref. 1). During the simulation the temperature used was kept small in relation to the excitation energy of the system; however, it had to be kept large enough so that the so-called ''sign problem'' did not become important. The sign problem arises only in fermion systems, as an odd permutation of the fermions results in the changing of the sign of the fermion density matrix, i.e., we have

$$\rho_F(R,R';\beta) = \frac{1}{N_S!} \sum_{\mathcal{P}} (-1)^{\mathcal{P}} \rho(\mathcal{P}R,R';\beta), \qquad (20)$$

where ρ_F is the fermion density matrix, $\beta = 1/kT$, N_S is the number of electrons in the specific spin state, $\mathcal{P}$ is the permutation operator of particle labels, and $R=\{\vec{r}_1, \ldots, \vec{r}_N\}$ is the set of all particle coordinates. This problem is explained in more detail by Fenghua and Ceperley.[17] In the position representation the Boltzmann density matrix ρ is defined as

$$\rho(R,R';\beta) = \langle R|e^{-\beta H}|R'\rangle. \qquad (21)$$

The density matrix can be expanded in terms of density matrices at higher temperatures, resulting in a good approximation as the system behaves classically at higher temperatures. Dividing up β in M ''imaginary time'' slices gives

$$\rho(R^0,R^M;\beta) = \int \cdots \int dR^1 dR^2 \cdots dR^{M-1} \times \rho(R^0,R^1;\tau) \cdots \rho(R^{M-1},R^M;\tau). \qquad (22)$$

Note $\tau = \beta/M = 1/k(MT)$, and MT becomes an effective temperature. Clearly this effective temperature can become much larger than the actual temperature when M becomes large.

As a numerical test for the system, we checked that there were only negligible deviations of the estimators calculated by the Monte Carlo simulation from the exact theoretical

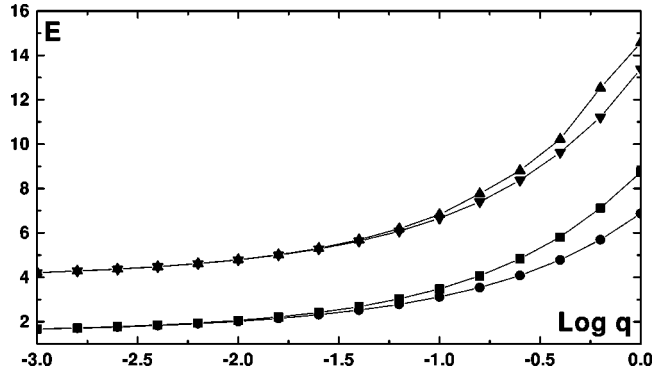

FIG. 8. Total energy of system vs the quantum parameter q. For $N=2$, $S=0$ is represented by circles and $S=1$ squares. For $N=3$, $S=1/2$ is represented by down triangles and $S=3/2$ up triangles. The smallest spin gives the lowest energy as $q\to 1$. The energy difference becomes extremely small for small values of q and the energies went slowly towards their classical values.

values (at the temperatures under consideration) for noninteracting fermions in a harmonic confinement. For example, the precision of the calculated energy was not worse than 0.5% (at the temperature at which the simulation was performed). All the configuration and thermodynamic properties were investigated as a function of the control parameter q. The values of q considered were between 10^{-3} and 1 and the temperature used was q dependent, but kept constant in oscillator units so that $kT=0.3\hbar\omega$.

This fermionic many-body formalism was used to obtain the values of the following quantities: (i) the total energy, E, (ii) the exchange energy, E_{exch}, (iii) the radial distribution of the particles $\rho(r)$, (iv) the half-height width of $\rho(r)$, Γ_{radial}, (v) the maximum position of $\rho(r)$, R_{radial}, (vi) the radius at which the pair correlation function $f(r)$ has a maximum, R_{pair}. For details about the derivations of these properties see, for example, Ref. 1 and references therein.

The total energy E was obtained by using the standard estimator:[18]

$$E=\left\langle \frac{3}{2}NT+\frac{1}{M}\sum_{i,m}\left\{-\frac{(R_i^m-R_i^{m-1})^2}{4q\tau^2}+\frac{1}{2}(R_i^m)^2\right\}+\frac{1}{M}\sum_{i<j,m}\frac{1}{|R_i^m-R_j^m|}\right\rangle, \tag{23}$$

where $\tau=\beta/M$, M is the number of imaginary time layers, and $1\leqslant m\leqslant M$. The first kinetic term follows from the equipartition theorem (using the dimensionless temperature, T). In our case $N=2$ or $N=3$. The negative part of the second term can phenomenologically be understood as a discrete approximation of the kinetic energy, using the imaginary time step $\Delta t=i2q\tau$. We have then roughly $E_{\mathrm{kin}}=qV^2=q(R^m-R^{m-1})^2/\Delta t^2=-(R^m-R^{m-1})^2/4q\tau^2$ (using dimensionless units).

The exchange energy E_{exch} is defined here as the fermionic total energy (the same as the total energy E) minus the corresponding Boltzmann energy (the energy in the case when the particles are distinguishable). The exchange energy serves here as an estimator of the transition between Wigner crystal and Fermi liquid and is directly connected with statistics. We also note that the mean number of particles that take part in particle permutations could be used for the same purpose. The maximum position of the (dimensionless) pair correlation function, R_{pair} describes the mean interparticle distance and can approximately be understood as the interparticle distance obtained in Sec. III with the mean value $(2b_1+b_2)/3$, where b_1 and b_2 are the distances in the triangle (See Fig. 1). In the limit $q\to 0$ the system is equivalent to the classical 3D Thomson atom (see Refs. 1 and 4 and references therein). For two electrons in the classical equilibrium state the electrons are located on the line going through the center of the confinement potential at the same separation from the center. Thus $R_{\mathrm{pair}}=1$ and the total energy $E=\frac{3}{2}$. Similarly for three classical electrons, the equilibrium state is when the electrons are located at the nodes of an equilateral triangle and $R_{\mathrm{pair}}=(\frac{3}{2})^{1/3}\approx 1.145$ and $E\approx 3.93$ [see Eq. (16)]. The Monte Carlo results are in agreement with these classical results, as shown below.

The radial distribution of the particles, $\rho(r)$, which is an analog to the reduced one-particle probability given in Sec. III [see Eq. (12)] averaged over the solid angle, gives information on status of the symmetry transformation. If there is a kink in the half-height width Γ_{radial} or in the maximum position R_{radial}, this indicates strongly a rapid symmetry change, or alternatively that the effects of the particle exchange start to become important. For the former case this is obvious if we take a look at Fig. 7. The radial distribution is simply an average over a ''circle'' in these figures. It can be seen that an angular average must change when the symmetry changes.

Finally we give here further details of the PIMC calculations. We performed the averaging as follows:

$$\langle A\rangle=\frac{1}{N_{\mathrm{eff}}}\sum p_iA_i, \tag{24}$$

where p_i is the parity of permutation i, where $p_0=1$, and $N_{\mathrm{eff}}=\Sigma p_i$ is the ''effective'' Markov chain length. Every permutation of two particles with the same spin changes the sign of the parity.

B. Results

The total energy, E is plotted in Fig. 8 for $N=2$ ($S=0$ and $S=1/2$) and $N=3$ ($S=1/2$ and $S=3/2$). The result for three electrons agrees strongly with the HF result. However, the energy crossover between the $S=1/2$ and the $S=3/2$ state cannot be observed as the numerical precision was not sufficient to determine the preferable spin state at the lower limit of q. Moreover, the temperature in the region of small values of q was still too high (e.g., compare with the energy difference in Fig. 5 of Sec. III). For $N=2$, however, there is no doubt that $S=0$ corresponds to the ground state, even at $T\neq 0$ K. It is easy to show that for two electrons, for this specific parabola problem, that $S=0$ always corresponds to the ground state for any temperature.

In Fig. 9, we plot the exchange energy, E_{exch} as a function of the control parameter q. It can be clearly seen that E_{exch} grows monotonically as q grows. Note also that the increase in E_{exch} starts at lower q and is larger in general for the higher spin states. For $N=3$ and $S=3/2$ it increases by up to 19% of the total energy at $q=10^0$, with a kink at $\log_{10}(q)=-1.75$. For two electrons the Fermi statistics starts to play a distinct role from $\log_{10}(q)\approx-1.25$. At this value of q, the exchange energy (which is directly connected with statistics) starts to increase as a function of q. As mentioned above the mean number of particles that take part in particle permutations gives an estimate of the importance of the Fermi statistics in the simulation to be made. The simulations show that this mean follows the same trend as the exchange energy. This is due to the fact that the permutations of the density matrix [given in Eq. (20), and needed to satisfy the total antisymmetry required by the Fermi statistics] have little effect for small values of q. As all statistical information is contained in this density matrix, the system becomes Boltzmann-like when q is small. However, this does not necessary mean that we can apply Fermi-Dirac statistics directly as the exchange starts to increase (since the particles still have non-negligible interactions, so that $E\neq\Sigma_j E_j$).

The radial distribution for two particles, $\rho(r)$, is plotted in Fig. 10 for different values of q in the spin state $S=1$. As can be seen, the distribution has a sharply localized shape for $q=0.001$, which gradually smooths out as q increases. We also see clearly that that the maximum moves towards the origin; as it becomes more broadly distributed. Thus, quantum ''melting'' occurs and the electrons are ''smeared'' out on the whole quantum dot. In other words, we have a transition from a Wigner crystal to a Fermi-liquid-like structure. To be able to resolve details in this transition we have calculated the half-height width, Γ_{radial} and the position of the maximum of $\rho(r)$, R_{radial}. In Fig. 11 the result of Γ_{radial} is plotted for as a function of q. For $N=2$ ($S=0$ and $S=1/2$) and $N=3$ ($S=1/2$ and $S=3/2$). For $N=3$, it has a kink at $\log_{10}(q)=-1.75$. This indicates an exchange effect and/or a symmetry transition. The maximum position, R_{radial}, however, which is plotted in Fig. 12 has a kink at $\log_{10}(q)=-1.25$. Therefore it seems likely that quantum melting occurs around these values of q. For $N=2$, there is no symmetry transition, so the kinks can only be explained as an exchange phenomena.

In Fig. 13, the position of the maximum of the pair correlation function, R_{pair} is plotted as a function of q. It can be interpreted as the mean interparticle distance. For $N=2$ we see that R_{pair} corresponds to the classical interparticle distance up to $\log_{10}(q)=-1.5$, where the different spin solutions start to diverge. Due to the additional statistical repulsion the mean interparticle distance for states with larger total spin increases more quickly as a function of q than states with smaller total spin because of the additional interelectron repulsion due to the exchange interaction. For $N=3$ the distance first decreases slowly, but then starts then to increase. For the $N=2$, $S=0$ state, however, the pair correlation function decreases monotonically. The nonmonotonic behavior is connected with Fermi statistics and is absent for

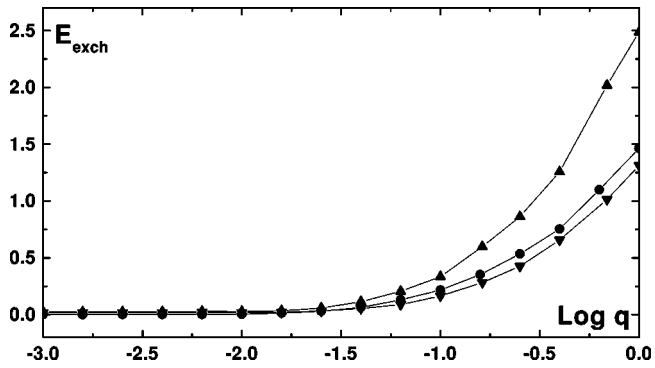

FIG. 9. Exchange energy of the system vs the quantum parameter q. For $N=2$, $S=1$ is represented by circles. For $N=3$, $S=1/2$ is represented by down triangles and $S=3/2$ up triangles. In general, the maximal spin gives maximal exchange.

Boltzmann systems. For small q the system is essentially equivalent to a Boltzmann system (due to the negligible overlapping of electron wave functions) and R_{pair} decreases with increasing q. As q is increased the role of the Fermi statistics becomes important and R_{pair} starts to increase with increasing q.

V. SUMMARY AND CONCLUSIONS

In this paper we present the results of PIMC and HF calculations for three electrons in a quantum dot (where the quantum dot is modeled by a harmonic potential). In addition, PIMC calculations were also performed for a two-electron system. The results for the different methods were found to be generally in agreement, but some differences were seen.

For the PIMC calculations on the two-electron system it was found that the spin state remained $S=0$ for all q and for $T\neq0$. The three-electron system, however, showed a number of phase transitions as q (and hence the confinement) was increased. Both methods predict a Wigner-crystal-like structure for weak confinement (i.e., small q). In this region the

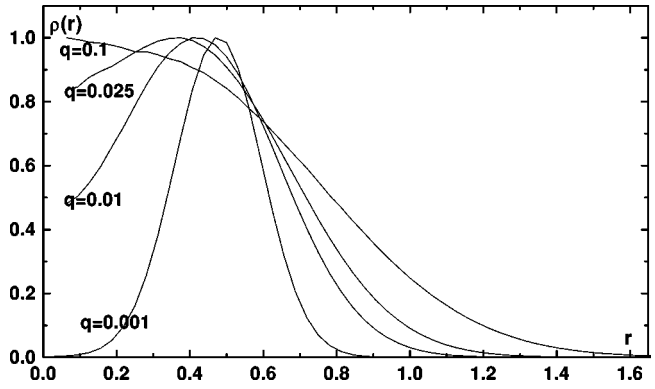

FIG. 10. Evolution of the radial distribution $\rho(r)$ with increasing q for $N=2$ and $S=1$. The electrons are sharply localized for $q=0.001$ and their structure corresponds to a Wigner crystal. As q increases, the position of the maximum moves towards the origin and the broadening becomes wider as well. The system behaves as a Fermi liquid in this region.

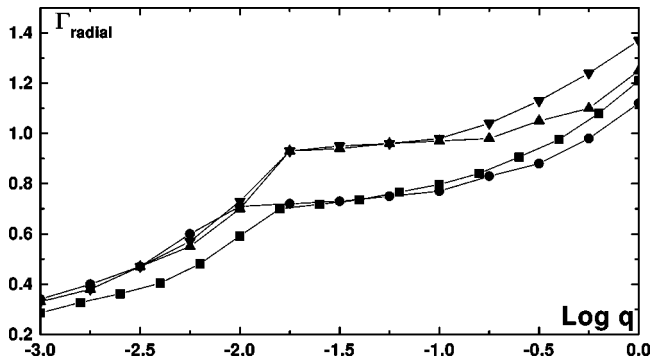

FIG. 11. Width of the radial distribution Γ_{radial} vs the quantum parameter q. For $N=2$, $S=0$ is represented by circles and $S=1$ squares. For $N=3$, $S=1/2$ is represented by down triangles and $S=3/2$ up triangles.

electrons form sharply peaked wave functions at the corners of an equilateral triangle. As the strength of the confinement increases ''cold'' or ''quantum'' melting takes place, and the electrons change from being strongly correlated to being weakly correlated. Related to this we found with the PIMC calculations that the particles considered were fermions, and hence obey Fermi statistics, which has an important effect on the properties of the system at large q.

The symmetry change is predicted more precisely by the HF method, as the strength of the confinement is increased and the symmetry of the system changes from C_3 to C_2 and finally to C_∞. The HF calculations also predict that the spin state will change from $S=3/2$ to $S=1/2$ at the same critical q value at which the transformation from C_3 to C_2 occurs. At a second critical q value the symmetry changes from C_2 to C_∞. The HF calculations also predict that a ''condensation'' phase transition will occur, within the spin state $S=3/2$ (even though the ground state is in the spin state $S=1/2$). These transitions cannot be seen with the PIMC method because (as can be seen from Fig. 8) there is only a small difference between the PIMC predicted energies of the $S=3/2$ state and the $S=1/2$ state for small q (see Fig. 5 as well), and the PIMC method is not precise enough to determine the lower-

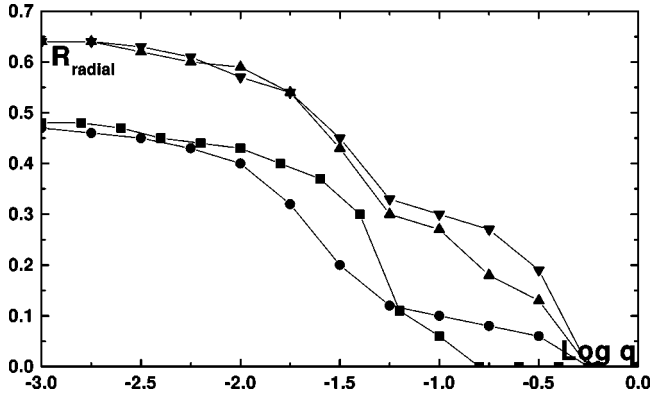

FIG. 12. Position R_{radial} of the maximum of the radial distribution vs the quantum parameter q. For $N=2$, $S=0$ is represented by circles and $S=1$ squares. For $N=3$, $S=1/2$ is represented by down triangles and $S=3/2$ up triangles.

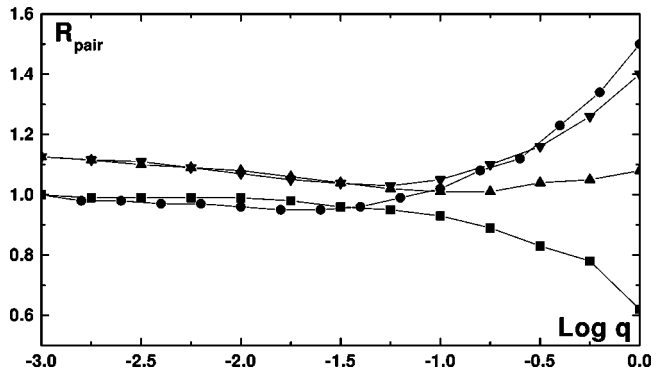

FIG. 13. Position R_{pair} of pair function maximum vs the quantum parameter q. For $N=2$, $S=0$ is represented by circles and $S=1$ squares. For $N=3$, $S=1/2$ is represented by down triangles and $S=3/2$ up triangles.

energy state, since the thermal energy is greater than the energy difference.

ACKNOWLEDGMENTS

The work was supported by INTAS, RFBRs, the Sweden Program, Quantum Devices, and SSF.

APPENDIX: EXPRESSIONS FOR $\langle H\rangle$ IN FERROMAGNETIC AND ANTIFERROMAGNETIC STATES

In this appendix we obtain expressions for the total energy of the system $E(b,\sigma)$ as a function of the variational parameters b and σ. The total energy of the system is defined as

$$E(b,\sigma)=\frac{\langle T\rangle+\langle U\rangle+\langle U_{ee}\rangle}{\langle\Psi|\Psi\rangle}. \tag{A1}$$

1. Ferromagnetic state $S=3/2$

First define J_{ij} as the overlap integral $\langle i|j\rangle$ between basis functions i and j. For C_3 symmetry (where the centers of wave functions are in corners of an equilateral triangle) all these overlap integrals are identical and can be denoted as simply J. Similarly for C_3 symmetry $b_1=b_2$ can be denoted as b. Hence we have

$$\langle\Psi|\Psi\rangle=(1-J^2)(1+2J). \tag{A2}$$

Now $J=\exp(-b^2/4\sigma^2)$. For the kinetic energy in the $|\uparrow\uparrow\uparrow\rangle$ state we obtain the following expression:

$$\langle T\rangle=\frac{3q}{2\sigma^4}(1-J)[b^2J^2+3\sigma^2(1+J-2J^2)]. \tag{A3}$$

Analogously we have the total confinement potential energy for this case:

$$\langle U\rangle=\frac{1}{2}[b^2(2+J^2(J-3))+9\sigma^2(1-J)^2(1+2J)]. \tag{A4}$$

Finally the Coulomb interaction between the different Gaussians is calculated as follows. The matrix elements

$$\Lambda_{i,j,n,m}=\int \frac{\phi_i(\vec{r}_1)\phi_j(\vec{r}_1)\phi_n(\vec{r}_2)\phi_m(\vec{r}_2)}{r_{12}}d\tau \qquad \text{(A5)}$$

and Gaussians $\phi_j(\vec{r}_i)$ with the same widths are calculated. We use the fact that a product of two Gaussians is also a Gaussian, apart from a factor. The interaction energy is then only dependent on the relative distance between the centers of these Gaussians and σ. The Coulomb interaction between two electrons, which are described by normalized Gaussians, separated a distance b, are given by the expression

$$U_{ee}=\frac{1}{\sigma}F(p), \qquad \text{(A6)}$$

where $p=b/\sigma$ and the function $F(p)$ is defined as the integral

$$F(p)=\frac{1}{p\sqrt{\pi}}\int_0^\infty e^{-(p+z)^2}(e^{4pz}-1)\mathrm{erf}(z)dz. \qquad \text{(A7)}$$

$F(p)$ was solved numerically for different p.

When $p\to\infty$ (in practice when $p\geqslant 5$), $F(p)\to 1/p$. With use of the definition of p we see that Eq. (A5) reduces in this case to the classical expression for interaction between two pointlike electrons. With use of Eqs. (A5) and (7) the total e-e interaction $\langle U_{ee}\rangle$ has the form

$$\langle U_{ee}\rangle=\frac{3}{\sigma}\left\{F(p)+2J^3F\left(\frac{p}{2}\right)-J^2\left[F(0)+2F\left(\frac{\sqrt{3}p}{2}\right)\right]\right\}. \qquad \text{(A8)}$$

Combining Eqs. (A1)–(A8) we obtain the expression for the ground-state energy $E_{\uparrow\uparrow\uparrow}$ as a function of the variational parameters b and σ.

2. Antiferromagnetic state $S=1/2$

For this state we have

$$\langle H\rangle=\frac{\langle\uparrow\uparrow\downarrow|H_0|\uparrow\uparrow\downarrow\rangle+\langle\uparrow\downarrow\uparrow|H_0|\uparrow\downarrow\uparrow\rangle+\langle\downarrow\uparrow\uparrow|H_0|\downarrow\uparrow\uparrow\rangle}{\langle\uparrow\uparrow\downarrow|\uparrow\uparrow\downarrow\rangle+\langle\uparrow\downarrow\uparrow|\uparrow\downarrow\uparrow\rangle+\langle\downarrow\uparrow\uparrow|\downarrow\uparrow\uparrow\rangle}. \qquad \text{(A9)}$$

Note that in Eq. (A9) the value of all the matrix elements in the numerator are the same, and similarly for the denominator. The components of Eq. (A9) are the following:

$$\langle U\rangle=\frac{1}{12}[2b_1^2(1-J_2)(4+J_1^2+4J_2)+b_2^2(4+J_1^2(4-J_2)+2J_2^2)+54\sigma^2(1-J_2)(1+J_1^2+J_2)], \qquad \text{(A10)}$$

$$\langle T\rangle=\frac{q}{4\sigma^4}[18\sigma^2(1-J_2)(1+J1^2+J_2)-2b_1^2J_1^2(1-J_2)+b_2^2J_2(J_1^2+2J_2)], \qquad \text{(A11)}$$

$$\langle U_{ee}\rangle=\frac{1}{\sigma}\left[2F(p_1)+F(p_2)+(J_1^2-J_2^2)F(0)+2J_1^2F\left(\frac{1}{2}\sqrt{p_1^2+2p_2^2}\right)\right]-\frac{J_2}{\sigma}\left\{J_1^2\left[2F\left(\frac{p_1}{2}\right)+F\left(\frac{p_2}{2}\right)\right]+2J_2F\left(\frac{1}{2}\sqrt{4p_1^2-p_2^2}\right)\right\}, \qquad \text{(A12)}$$

$$\langle\Psi|\Psi\rangle=(1-J_2)(1+J_1^2+J_2), \qquad \text{(A13)}$$

where $p_1=b_1/\sigma$, $p_2=b_2/\sigma$, $J_1=\exp(-b_1^2/4\sigma^2)$, and $J_2=\exp(-b_2^2/4\sigma^2)$.

*Email address: sunkan@fy.chalmers.se

[1] A.V. Filinov, Yu.E. Lozovik, and M. Bonitz, Phys. Rev. Lett. **86**, 3851 (2001); Yu.E. Lozovik, Usp. Fiz. Nauk **153**, 356 (1987); Yu.E. Lozovik and V.A. Mandelshtam, Phys. Lett. A **165**, 468 (1992); N.E. Kaputkina and Yu.E. Lozovik, Phys. Solid State **40**, 1594 (1998); *ibid.*, **40**, 1935 (1998). See also the analysis of classical 3D Coulomb cluster by Yu.E. Lozovik and V.A. Mandelshtam, Phys. Lett. A **145**, 269 (1991); Yu.E. Lozovik and E.A. Rakoch, *ibid.* **235**, 55 (1997).

[2] B. Reusch, W. Hausler, and H. Grabert, Phys. Rev. B **63**, 113313 (2001); R. Egger, W. Hausler, C.H. Mak, and H. Grabert, Phys. Rev. Lett. **82**, 3320 (1998).

[3] C. Yannouleas and U. Landman, Phys. Rev. Lett. **85**, 1726 (2000); **82**, 5325 (1999); C. Yannouleas, Phys. Rev. B **61**, 15 895 (2000).

[4] N.A. Bruce and P.A. Maksym, Phys. Rev. B **61**, 4718 (2000).

[5] R. Egger, W. Hussler, C.H. Mak, and H. Grabert, Phys. Rev. Lett. **82**, 3320 (1999); **83**, 462(E) (1999).

[6] S.M. Reimann, M. Koskinen, and M. Maninen, Phys. Rev. B **62**, 8108 (2000).

[7] B. Meurer, D. Heitmann, and K. Ploog, Phys. Rev. Lett. **68**, 1371 (1992).

[8] R.C. Ashoori, Nature (London) **379**, 413 (1996).

[9] Yu.E. Lozovik and V.I. Yudson, Zh. Eksp. Teor. Fiz. Pis'ma Red. **22**, 556 (1975); N.E. Kaputkina and Yu.E. Lozovik, Phys. Scr. **22**, 556 (1975).

[10] L. Jacak, P. Hawrylak, and A. Wójs, *Quantum Dots* (Springer Verlag, Heidelberg, 1998).

[11] T. Chakraborty, *Quantum Dots* (Elsevier, Amsterdam, 1999).

[12] U. Merkt, J. Heuser, and M. Wagner, Phys. Rev. B **43**, 7320 (1991).

[13] K. Hirose and N.S. Wingreen, Phys. Rev. B **59**, 4604 (1999).

[14] J. Harting, O. Mülken, and P. Borrmann, Phys. Rev. B **62**, 10 207 (2000).

[15] W. Pauli, Z. Phys. **43**, 610 (1927).

[16] S. Tomonaga, *The Story of Spin* (University of Chicago Press, cop., 1997), p. 54.

[17] Z. Fenghua and D.M. Ceperley, Phys. Rev. E **58**, 5123 (1998).

[18] D.M. Ceperley, Rev. Mod. Phys. **67**, 279 (1995).